Comparative Experimental and Numerical Evaluation of the Flow Field at the Stern of a Hull Form

Dimitris Liarokapis *, Gregory Grigoropoulos, George Tzabiras

Posted Date: 1 April 2026

doi: 10.20944/preprints202604.0010.v1

Keywords: flow field evaluation; 5-hole tube calibration; towing tank wake field measurement; CFD flow around ship models; CFD methods for ship propulsion

 doi:10.20944/preprints202604.0010.v1

Article

Comparative Experimental and Numerical Evaluation of the Flow Field at the Stern of a Hull Form

Dimitris Liarokapis *, Gregory Grigoropoulos and George Tzabiras

Laboratory for Ship and Marine Hydrodynamics, National Technical University of Athens, Zografou Campus, 9 Hroon Polytechneiou Str, 15 772, Zografou, Athens, Greece

* Correspondence: dliaro@central.ntua.gr

Abstract

The basic aim of this research was to compare the experimentally evaluated flow field at the stern region of a hull form with large block coefficient with the respective numerical results. To this end, a Five-Hole Pitot tube was used to capture the wake flow at the stern region of a scaled model of a bulk carrier in the towing tank of the Laboratory for Ship and Marine Hydrodynamic (LSMH) of the National Technical University of Athens (NTUA). The measurements were carried out at three aft sections of the model, where large scale vortices are usually generated: the section at the propeller, a section ahead of it and another one under the transom stern. The model was towed at a speed of 1.214 m/s, corresponding to Fn =0.17. The tube was calibrated on air at an equivalent Re, while a second in-house calibration technique was developed to consider installation misalignments and to increase overall measurement accuracy. The numerical calculation of the flow was performed using CFD tools developed at LSMH of NTUA. The method solves the RANS equations by applying the finite volume approach underneath a prescribed free surface which is derived by a potential flow code. The numerical results are in good agreement with the experimental ones, confirming the robustness of both methods.

Keywords: flow field evaluation; 5-hole tube calibration; towing tank wake field measurement; CFD flow around ship models; CFD methods for ship propulsion

1. Introduction

The flow field around a sailing ship strongly affects both its resistance and the performance of the propulsion system. Accurate flow-field recordings are of great importance for the design of a hull form, since they can be used to optimize its shape and properly locate its appendages. Especially at the stern region of bulky hull forms, where the flow varies intensively, the robust evaluation of the turbulence in the wake is fundamental for the proper design of the propulsion system. To be more specific, the determination of the nominal wake field in the absence of the propeller is of crucial importance for the propeller design [1]. In this study we will present comparison between numerical calculations and five-hole Pitot measurements concerning three sections at the stern of a bulk carrier model.

A Five-hole Pitot tube system was designed, implemented and tested at the LSMH of NTUA [2]. The experimental method used is well established and highly reputable because of its accuracy and reliability but not trivial. In this sense, it is utilized not only for direct flow field investigations, but also as a reference method for the validation of numerical and PIV methods. The prerequisites for accurate and reliable measurements, as well as the limitations of the method will be discussed in detail.

There are various experimental methods to measure the velocity of the fluid in a specific point or a range of points of the flow field. Some of them measure the 2D flow on a transverse plane, while the full 3D records of the flow field are obtained using most of the concepts. The available methods can be grouped into two major categories, the intrusive and non-intrusive.

 doi:10.20944/preprints202604.0010.v1

The non-intrusive methods employ emitted radiation (Laser Doppler Velocimetry (LDV), Particle Image Velocimetry (PIV), Ultrasonic waves, Electromagnetic etc. and analyze the reflection. This approach provides significant flexibility and convenience but suffers from scrambles and complexities in the analysis of the reflection. On the other hand, intrusive methods (Multi-Hole Probes, Hot Wire Anemometry (HWA)), which are mainly based on the concept of Pitot tube, have great accuracy and reliability, as they preserve in a satisfactory low level the disturbance of the instrument intrusion to the flow at the point of interest [3].

Pitot tube measurements comprise the second most popular method for obtaining the flow velocity field in laboratory facilities such as the towing tank. Particle Image Velocimetry (PIV) is the most popular method used in numerous experimental studies of the wake field of ship models [4–7]. Particle Image Velocimetry (LDV) [8–10], that records the instantaneous velocity vector at a single point with a relatively high frequency is the most accurate method. Acoustic Doppler Velocimetry (ADV) is another popular method for accurate measurements.

Nevertheless, performing towing tank tests preserve always a degree of uncertainty (owing to scale effects). Therefore, it is not certain that they will lead on the safe evaluation and the ship's performance may be miscalculated. To improve such predictions numerical simulation tools that resolve the self-propulsive ship (CFD) may be used as an alternative valuable tool [11].

In our case, the numerical calculations were produced by applying CFD tools that have been developed at LSMH of NTUA. The basic method is a hybrid process that solves the RANS equations by applying the finite volume approach in a restricted computational domain underneath a prescribed free surface which is determined through a potential flow code [12].

Both numerical and experimental methods have been used to acquire the flow filed at three sections at the stern of a bulk-carrier model sailing at service speed for one loading and trim condition. The aim of the present study is to demonstrate the possible benefits of such methodologies to avoid any undesired inaccuracies.

2. Concept of Pitot Tube

The concept of measuring static and stagnation pressure originates from the energy conservation law, which correlates pressure and velocity and provides the engineers with a useful tool to calculate velocity profile by measuring the pressure field [13]. By measuring the dynamic pressure at a single point, the fluid velocity can be calculated using Bernoulli's equation. Basic condition is that the tube will be placed parallel to the flow. Thus, the experimentalist must know the flow direction a priori.

A more sophisticated version of these tubes is the multi-hole probes that can measure the magnitude and the direction of the flow at incidence angles up to 75 degrees (velocity vector). Thereafter multi-hole Pitot tubes are introduced for enhanced flexibility in the alignment requirements and for fully 3D measurements. The main difference between the five-hole and seven-hole probes is the angular resolution capability [14–16]. Multi-hole probe is a single point, intrusive instrument, and thus, it has certain limitations on its use. Special attention must be paid so that the tube itself does not alter the flow significantly at the measuring point. Especially, in towing tank measurements the probe must not be positioned close to the model surface or other solids that interfere with the flow.

2.1. Principles of Pitot Tube

The velocity of the fluid is calculated from the measurement of the differential pressure between the direct flow pressure and the static pressure ports. This type of Pitot tube is known as a Pitot-static tube because the static pressure is also measured within the same measurement head.

In its basic form, the tube is placed parallel to flow. At the tip of the probe (impact pressure port) that is called the stagnation point the manometer measures the total pressure (Figure 1). By assuming that the fluid is in a steady state, for the closed system there is a conservation of energy along the flow line. This was first described by Daniel Bernoulli in 18th Century.

 doi:10.20944/preprints202604.0010.v1

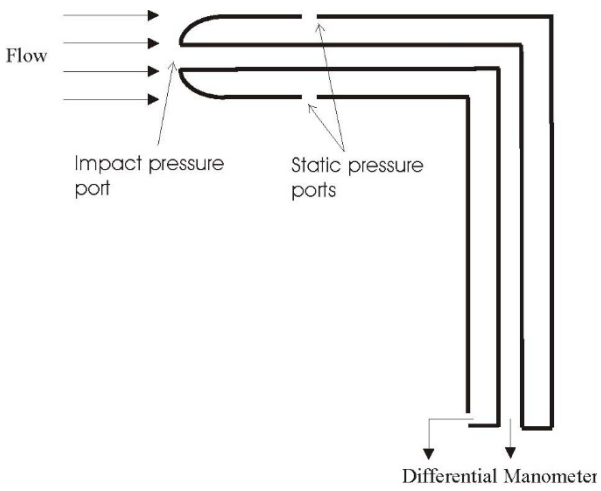

Figure 1. Principles of Pitot Tube.

The Bernoulli equation describes a non-turbulent, perfect, incompressible, and barotropic fluid undergoing steady motion. Several forms of the equation can be derived, depending on assumptions and simplifications made about the fluid flow. One of the common forms of Bernoulli's Equation used for Pitot tube measurements is the following expression:

$$\frac{V^2}{2g} + \frac{P}{\rho g} = C \quad (1)$$

where V, P and ϱ is the velocity, the pressure and the density of the fluid respectively, g = 9.81 m*s^{-2}, is the gravity acceleration and C is a constant over a streamline. Applying the above equation at the tip of the probe (V2, P2) and at the static ports (V1, P1) the above equation becomes as follows:

$$\frac{V_1^2}{2g} + \frac{P_1}{\rho g} = \frac{V_2^2}{2g} + \frac{P_2}{\rho g} \quad (2)$$

But, at the tip of the probe, the velocity of the fluid becomes zero. Thus:

$$\frac{V_1^2}{2g} + \frac{P_1}{\rho g} = \frac{P_2}{\rho g} \quad (3)$$

or

$$V = \sqrt{\frac{2\Delta_P}{\rho}} \quad (4)$$

where Δp is the dynamic pressure, which is the pressure difference between the stagnation pressure tap and the static pressure tap.

We must keep in mind that equation 4 is valid only if the fluid is incompressible, non-viscous, the temperature is constant and the two points of measurements are in the same streamline. If these pressures are measured accurately by the traducer, then the velocity of the fluid can be estimated.

In practice, any imperfection on the design and manufacture process will alter the desired outcome, thus all tubes are calibrated against a reference Pitot tube. Moreover, most of the assumptions made when applying Bernoulli's equation are not always correct. The effect they have on the results cannot be estimated accurately [17]. All relative assumptions will be discussed in the following paragraphs.

3. CFD Theoretical Background

Computations around the model hull follow a hybrid two-stage approach which has been developed in the Laboratory of Ship and Marine Hydrodynamics of NTUA. At first, the free-surface

 doi:10.20944/preprints202604.0010.v1

geometry around the hull is calculated according to a hybrid method which combines the potential flow solver of [18] around the bow region with the viscous flow code at the stern and wake regions, as described in [19]. Then, under the known free surface, the RANS equations are solved in a restricted domain to achieve, as far as possible, accurate results.

A three-block arrangement is followed that allows for very fine grid resolutions applied, as shown on Figure 2. In block (I) covering the bulbous bow area and a portion of the middle part a combination of A C-O type and an H-O type grid are generated following the conformal mapping technique proposed in [20]. Block (II) consists of an H-O grid formed by the same procedure and covering the stern part up to the model aft end, while near the transom and in the wake region an H-H type Cartesian grid is adopted. The RANS equations are solved using an orthogonal curvilinear system (xi, xj, xl) with metrics (hi, hj, hl) and velocity components (ui, uj, ul) [21]. Then, the ui-momentum equation reads:

$$C(u_i) = -\frac{1}{h_i}\frac{\partial p}{\partial x_i} + \rho u_j^2 K_{ji} + \rho u_l^2 K_{li} - \rho u_i u_j K_{ij} - \rho u_i u_l K_{il} + (\sigma_{ii} - \sigma_{jj}) K_{ji} + (\sigma_{ii} - \sigma_{ll}) K_{li}$$
$$+ \sigma_{ij}(2K_{ij} + K_{ij}) + \sigma_{il}(2K_{il} + K_{jl}) + \frac{1}{h_i}\frac{\partial \sigma_{ii}}{\partial x_i} + \frac{1}{h_j}\frac{\partial \sigma_{ij}}{\partial x_j} + \frac{1}{h_l}\frac{\partial \sigma_{il}}{\partial x_l} \quad (5)$$

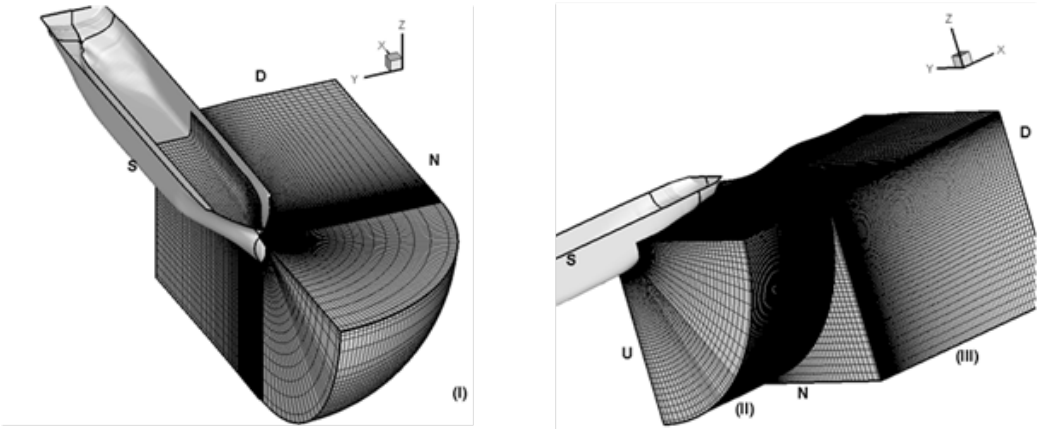

(**a**) (**b**)

Figure 2. (**a**) C-type grid formation about a bulbous bow (Block I); (**b**) H-O type grid in blocks II and III.

In the above equation, Kij stands for the curvature, ϱ for the fluid density, p for the static plus the hydrostatic pressure and σij are the stress tensor components. The other two momentum equations are derived by cyclic permutation of indices (i, j, l). The convective part on the l.h.s. of Equation 5 is written for any scalar variable Φ as:

$$C(\Phi) = \frac{\rho}{h_i h_j h_l}\left[\frac{\partial(h_j h_l u_i \Phi)}{\partial x_i} + \frac{\partial(h_i h_l u_j \Phi)}{\partial x_j} + \frac{\partial(h_i h_j u_l \Phi)}{\partial x_l}\right] \quad (6)$$

The stress tensor components are computed by adopting the eddy viscosity concept as:

$$\sigma_{ii} = 2\mu_e e_{ii} = 2\mu_e\left[\frac{1}{h_i}\frac{\partial u_i}{\partial x_i} + u_j K_{ij} + u_l K_{il}\right]$$
$$\sigma_{ij} = \mu_e e_{ij} = \mu_e\left[\frac{h_j}{h_i}\frac{\partial}{\partial x_i}\left(\frac{u_j}{h_j}\right) + \frac{h_i}{h_j}\frac{\partial}{\partial x_j}\left(\frac{u_i}{h_i}\right)\right] \quad (7)$$

In the above equation, the effective viscosity μe is calculated according to the SST-k-ω turbulence model of Menter [22] by solving two more differential equations, one for the kinetic energy of turbulence k and the other for the specific dissipation rate ω:

 doi:10.20944/preprints202604.0010.v1

$$C(k)=$$
$$\frac{1}{h_i h_j h_l}\left[\frac{\partial}{\partial x_i}\left(\sigma_k \mu_t \frac{h_j h_l}{h_i}\frac{\partial k}{\partial x_i}\right)+\frac{\partial}{\partial x_j}\left(\sigma_k \mu_t \frac{h_i h_l}{h_j}\frac{\partial k}{\partial x_j}\right)+\frac{\partial}{\partial x_l}\left(\sigma_k \mu_t \frac{h_i h_j}{h_l}\frac{\partial k}{\partial x_l}\right)\right] \quad (8)$$
$$+G-\beta^{*}\rho\omega k$$

$$C(\omega)=$$
$$\frac{1}{h_i h_j h_l}\left[\frac{\partial}{\partial x_i}\left(\sigma_\omega \mu_t \frac{h_j h_l}{h_i}\frac{\partial \omega}{\partial x_i}\right)+\frac{\partial}{\partial x_j}\left(\sigma_\omega \mu_t \frac{h_i h_l}{h_j}\frac{\partial \omega}{\partial x_j}\right)+\frac{\partial}{\partial x_l}\left(\sigma_\omega \mu_t \frac{h_i h_j}{h_l}\frac{\partial \omega}{\partial x_l}\right)\right] \quad (9)$$
$$+\frac{\gamma}{v_t}G-\beta\rho\omega^2+2\rho(1-F_1)\frac{\sigma_\omega}{\omega}\frac{1}{h_j^2}\frac{\partial k}{\partial x_j}\frac{\partial \omega}{\partial x_j}$$

The generation term G of turbulence in Equations 8, 9 is defined as:

$$G=2\mu_t\left[e_{ii}^2+e_{jj}^2+e_{ll}^2+\tfrac{1}{2}\left(e_{ij}^2+e_{il}^2+e_{jl}^2\right)\right] \quad (10)$$

The eddy viscosity μ_t as a function of k and ω as well as the constants and the blending function F1 appearing on the r.h.s. of Eqs. 7, 8 and 9 are defined in the original paper of Menter [22].

The numerical method to solve equations (5) and (8, 9) is based on the control volume approach by adopting a staggered grid system [20]. Second order approximation is applied for diffusion and spatial derivatives, while convection terms are modeled by the upstream second order scheme in conjunction to the min-mod limiter. A SIMPLE-type algorithm is applied to solve the pressure field. In all examined problems the numerical solution is completed by performing several sweeps of the domain until convergence is achieved.

The boundary conditions on solid boundaries follow the wall function approach, while Neumann-type conditions are applied on the flow-symmetry planes. On the free surface, the kinematic condition is applied for the velocity components, and the pressure is determined through the Neumann condition, since the dynamic condition is implied in the employment of a fixed boundary.

Dirichlet conditions are applied on the external boundary N (Figure 2), by calculating the velocity components and the pressure from the potential flow solution around the hull and beneath the specified free surface. Open-type conditions are adopted at the downstream plane D of block III [21], whereas in the three-block arrangement of Figure 2, the variables on the matching planes of blocks II and III are calculated by linear interpolations. The solution is completed first in block I while blocks II and III are solved simultaneously. Grid dependence tests performed in [23] about the same model have shown that an application of a 15.8M grid points in the computational domain about the hull produces satisfactory results for the total resistance and, therefore, he same grid has been adopted to compare the computational to the measured velocity components in the present work.

4. Implementation of the Multi-Hole Pitot tube

Pitot-tube systems are relatively simple and inexpensive compared to a modern PIV system for underwater measurements. However, to ensure the accuracy and flexibility of the measurements a series of auxiliary systems are necessary, which increases both the cost and the complexity of the complete arrangement [3]. The system layout of LSMH configuration (Figure 3) consists of five basic components, the multi-hole Pitot tube, the pressure sensors with the bleeding valves, the data acquisition, the traversing mechanism and the software to analyze the data.

 doi:10.20944/preprints202604.0010.v1

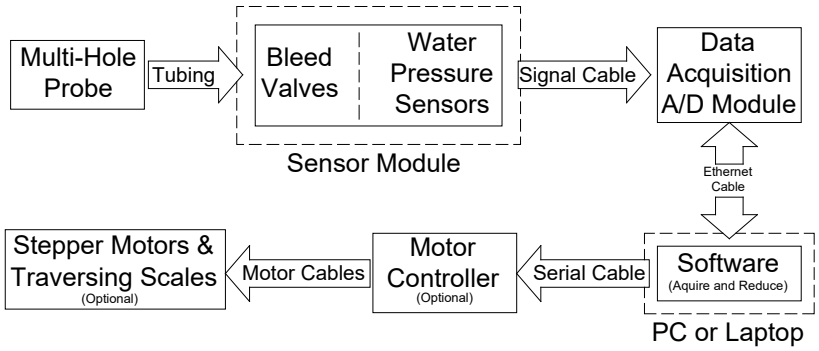

Figure 3. System Layout.

More specifically, the LSMH system consists of the following parts:

- A multi-hole Pitot tube probe;
- Pressure sensors, dedicated to measured fluid and the expected pressure range;
- Data acquisition hardware and software tied with pressure sensors;
- Pressure-to-velocity conversion software taking in to account calibration tables; and
- Traverse mechanism to precisely position the probe within all directions of a Cartesian coordinate system with feedback;
- Accurate probe calibrations within the expected speed range of the flow field are carried out prior to experiments

4.1. Pitot Tube Selection

The LSMH designed in collaboration with Aeroprobe Corporation a Five-Hole tube, suitable for underwater measurements (Figure 4). The main effort focused on the probe geometry, to keep the flow disturbance the lowest possible. Based on the above and considering the average size of LSMH models (3-5 m) the overall length of the probe was set to 50 cm. The tip diameter of the probe was selected at 8 mm and new inner tube diameter at 1.3 mm. The range of this instrument is limited to velocity vectors inclined by less than 55 – 60 degrees with respect to the probe axis [24]. However, the expected angles of the flow at the experiments were within this range.

Typical towing tank measuring time is usual limited. The real time dynamic response of the system is very crucial to ensure precise readings. Normally there is a need for a long set of measurements for every speed, while the available measuring time per run is limited. Internal tube diameter, tube length, the volume of the chamber of the pressure sensor used and air bubbles trapped in the system, significantly affects the response of the system.

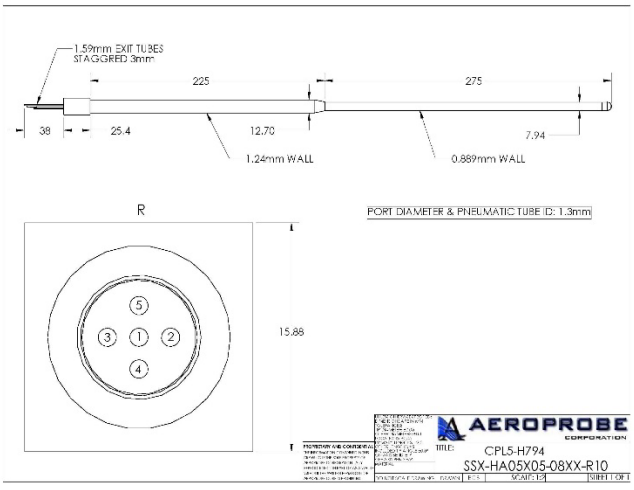

 doi:10.20944/preprints202604.0010.v1

Figure 4. 5-Hole Pitot tube designed in collaboration with Aeroprobe for the demands of LSMH.

To investigate the influence of the inner tube diameter to the response time, an experimental apparatus was prepared, using medical stainless tubes with internal diameter ranging from 0.4 mm to 0.8 mm and overall length of 50 mm. The tests revealed that the response time is strongly affected by the inner tube diameter (Table 1). Slow responses can be attributed to capillary phenomena.

Following the results from Table 1, tube with 1.3 mm inner diameter was selected (minimum inner tube diameter should not be lower than 0.8 – 0.9 mm). In the following table, the response time for several inner tube diameters is presented.

Table 1. Tube Inner Diameter vs Response Time.

Inner Tube Diameter (mm)	Response Time (sec)
0.4	> 20
0.5	7-8
0.6	5
0.7	3-3.5
0.8	2
0.9	<1
1.0	ms

4.2. Pitot Tube Calibration

An accurate probe calibration is required to encompass the expected speed ranges of the probe. Geometrical defects of the probe are considered during the calibration. Accuracy is typically better than 1% of the flow speed and 0.5 degrees in flow angles [25–27]. The probe is calibrated in a wind tunnel at multiple flow angles in an airstream of constant speed [28]. The probe is mounted on a positioning mechanism, capable of independent movement of the probe in two degrees of freedom at various yaw and pitch angles. Subsequently, a system of stepper drive motors positions the probe to a series of predetermined positions and orientations with respect to the free stream. The aim of this procedure is to correlate systematically the five pressure readings from the corresponding taps with the alteration of the velocity heading angle.

In our case, the calibration procedure was divided into two stages. Initially the first calibration was conducted in air at equivalent Reynolds number at three Mach numbers, 0.045, 0.130 and 0.220 equivalents to 1, 3 and 5 m/s towing speeds at the temperature of 20 degrees. This procedure was performed by the probes manufacturer (AeroProbe Coorp.). Calibrations at additional flow speeds are used to interpolate test data between calibration maps.

The probe calibration was a set of coefficients that used the probe pressures to calculate angle of attack (α), sideslip angle (β), stagnation pressure, static pressure and dynamic pressure. By knowing the fluid temperature (density) the velocity vectors at each point can be calculated. For a five-hole pitot, only four coefficients, two for the pitch and yaw angle and two for static and total pressure, were sufficient to calculate the velocity vector.

In practice, a reduction method was used. Three differential sensors measure the pressure differences ($P_{central}$-P_{static}, P_{left}-P_{right} and P_{top}-P_{bottom}). In this method the flow is assumed to be incompressible, which is the case we have investigated. The procedure started by calculating the Q_{bar}, C_a, C_b and Cq coefficients from the following equations:

$$Q_{bar} = P_1 - P_6 \quad (11)$$

$$C_a = (P_4 - P_5)/ Q_{bar} \quad (12)$$

$$C_b = (P_2 - P_3)/ Q_{bar} \quad (13)$$

 doi:10.20944/preprints202604.0010.v1

$$C_q = (P_1 - P_6)/ P_t \quad (14)$$

Next, the values of Ca and Cb are plotted against the calibration angles. The same procedure was repeated for Cq coefficient. By fitting a polynomial equation to the data, the polynomial coefficients are calculated.

$$a = C_0+C_1*C_\alpha+C^2*C_\alpha^2+C_3*C_\alpha^3+C_4*C_\alpha^4, \text{ and} \quad (15)$$

$$b = C_0+C_1*C_\alpha+C_2*C_\alpha^2+C_3\cdot C_\alpha^3+C_4*C_\alpha^4 \quad (16)$$

The coefficient Cq relates the velocity to the angle, and Ca or Cb are the non-dimensional angle coefficients. By using the polynomial coefficients we can calculate the alpha and beta angles from the pressure readings.

The second procedure involved the re-calibration of the probe in the towing tank of LSMH. The probe was attached to a position mechanism, allowing accurate rotation of the probe around the lateral and vertical axis. Initially, the probe was aligned to the lateral and longitudinal axis of the towing tank. Then, the probe was calibrated against a grid of known preset angles in the horizontal plane at the model test speed. The second calibration revealed an average percentage overestimation of about 5% for the velocity magnitude and angle declination of +- ±1.5 degrees when air calibration files were used. By the measured pressure data, the Ca, Cb and Cq coefficients were recalculated. By recalibrating the probe, small misalignments, different pressure sensors, tubing and geometrical imperfections were considered, increasing the overall accuracy substantially.

4.3. Pressure Sensor Selection

The range of the selected pressure sensors is crucial for the overall accuracy of the measurement. It is of great importance at the design stage to estimate the maximum and lower pressure readings expected. By conducting open water test trials with the probe in upstream position, a minimum pressure difference of 1.38 mbar was recorded at the side holes of the probe. To ensure sufficient accuracy, differential sensors within the range of 70 mbar with 0.25% accuracy and 2ms response time were selected.

The typical situation in the towing tank is to have low static pressure compared to the atmospheric. The magnitude of the difference between the atmospheric and the static pressure is of higher order than the expected measuring alterations (Figure 5). Thus, the atmospheric pressure should not be used as a reference pressure. To overcome this issue, either the pressure sensors should be located as close to the free surface as possible, or a reference pressure should be adjusted between the local ambient pressure and the total probe water pressure by a custom apparatus.

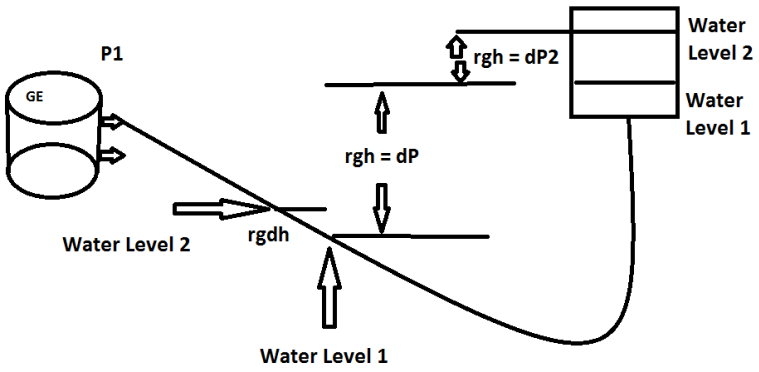

P1 = P0 + rgdh but if we calculate only the dP2 then we include rgdh in the calibration, so dP2 is the corect reading

 doi:10.20944/preprints202604.0010.v1

Figure 5. Principles of Pressure Reading.

4.4. Traversing System

To measure the flow field at the wake of a bulk carrier ship, an integrated system consisting of a 3-D traversing sub-system and a multi-hole Pitot tube was designed and implemented in the towing tank of LSMH (Figure 6). The traversing system consists of three linear traversing beams, capable of scanning a predefined grid of points at the desired plane of interest. The motion is controlled by two VXM controllers (Velmex Inc.) linked together offering the ability to move simultaneously along the three axes. Reliable performance is achieved with a powerful RISC Microcontroller that directly controls the phase of the motor using an optimized modulated method to produce resonance-free motor torque.

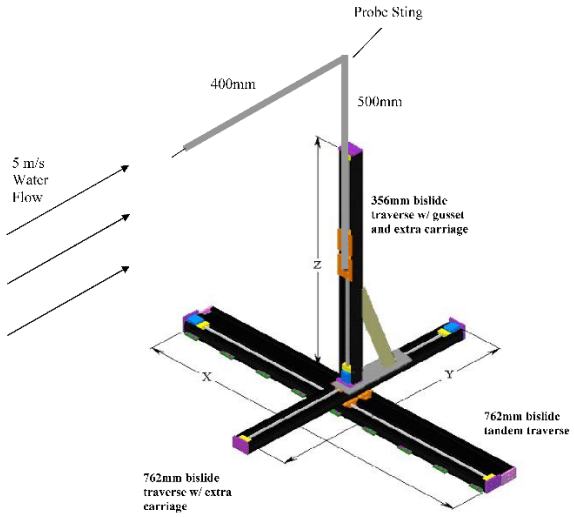

Figure 6. 3D traversing system.

5. Test Procedure

All experiments were conducted in the towing tank of the Laboratory of Ship and Marine Hydrodynamic of National Technical University of Athens (NTUA), measuring 100m in length, 4.53 m in width and about 3 m in depth. Wave absorbers were arranged along the sides of the tank to reduce waiting time between the experiments.

5.1. The Model Tested

The model used at the experiments corresponded to B/C HURON, a bulk carrier with a bulbous bow and transom stern. The length of the model was 5.110 m and its scale λ = 1:35. A turbulence stimulator was fitted to the model accordingly to the ITTC guidelines. The model was tested at the draft of 0.207 m, at even keel condition and at model speed of V = 1.217 m/s, corresponding to a Froude number of 0.17. The selected speed corresponds to the service speed of the vessel. Measurements duration was set to 40 seconds, at a sampling rate of 50 Hz. All the experiments were conducted without the propeller and the rudder fitted on the model. The main particulars of the model are listed on Table 2.

Table 2. Main particulars of B/C HURON at model scale.

Main Particulars		
Length at waterline,	L_{WL}	5.139 m
Breadth at waterline,	B_{WL}	0.677 m
Draft at midship,	T_M	0.207 m

 doi:10.20944/preprints202604.0010.v1

Displacement,	Δ	591.5 kg
Trim,	t	Even keel
Wetted surface area,	WS	4.67 m^2
Long. centre of buoyancy,	LCB	0.113m

6. Measuring Errors

In the present study, it was hard to estimate the total errors of the measurements. The total error analysis incudes the uncertainty of the pressure transducer calibration, the uncertainty of the pitot tube calibration and the uncertainty in the measurement of the flow angle and velocity magnitude by using the calibrated system. It must be stated that the positioning of the probe in the wake of the model augmented the uncertainty estimation to a very complex task. Nevertheless, the hydrodynamic effects (Reynolds number, viscous flows) were disregarded.

An attempt to minimize the sources of uncertainty was made. The accuracy of the pressure sensors was sufficient for accurately measuring the pressure differences appearing at the wake of the model. The positioning device had a maximum error in positioning of 0.01 mm. The sampling rate was chosen to be 10 times higher than the frequency of the expected phenomenon. It should be mentioned that repetitive tests could not were performed due to the limited time available in the towing tank.

Aeroprobe Company provided a first estimate of the errors (Table 3) following the air calibration of the probe. After the calibration the probe was placed in a known flow (velocity) at accurately specified angular positions. The outcome from the calibration functions was compared with the known input values.

Table 3. Error Estimation provided by Aeroprobe Company.

M=0.045	**Beta Bias**	**Beta 2σ**	**Beta Err.**	**Beta Vel. Bias**	**Beta Vel. 2σ**	**Beta Vel. Er.**
Main	0.005	0.113	0.118	0.015	0.218	0.234
Extended	-0.006	0.436	0.442	-0.018	0.239	0.257
	Alpha Bias	**Alpha 2σ**	**Alpha Err.**	**Alpha Vel. Bias**	**Alpha Vel. 2σ**	**Alpha Vel. Er.**
Main	0.002	0.123	0.125	0.011	0.226	0.237
Extended	-0.002	0.447	0.449	-0.013	0.279	0.291

The above probe calibration was valid for air measurements conducted at the test rig of the Aeroprobe Company. However, an average percentage declination of about 1% for the velocity magnitude and ±1.5% for the angle declination was measured in the water, even after recalibrating the probe. Compared to the eror estimations provided by Aeroprobe Company, the error was significantly higher. In contrast, it was comparable to the estimation of published data by other institutions conducting similar measurements in water. Probably, the sources of the errors include flow instabilities, blockage, position errors, vibrations from the carriage, etc. In any case, the errors at the angle estimation were much higher than the estimation for the flow velocity.

7. Analysis and Presentation of the Results

Three sections at the stern of the model were investigated acquiring approximately 300 measuring points on every section. Reference depth for the pitot measurements was set at 1.4 cm below the water surface, while the respective reference level for the analytical method (CFD) was set at the upper point of the transom resulting to a height difference of 20 cm between the two Z-axis origins.

It should be noted that the measurement were performed at the half width of the ship, as it is axisymmetric.

 doi:10.20944/preprints202604.0010.v1

7.1. Transom Section

The first section investigated, located right under the transom of the model. A rectangular grid 35 cm by 35 cm starting 1.4 cm below the water surface at the midpoint (symmetry plane) of the model was measured. The step between the measured points was set to 2 cm. Approximately 290 points were measured on this section. The density is considered sufficient, since each point corresponded to one carriage measurement.

The velocity vectors under the transom of the model are plotted in Figures 7a and 7b. Moreover, the iso-contours where the velocity ratio (V measured over axial velocity) is constant are presented in Figures 8a and 8b.

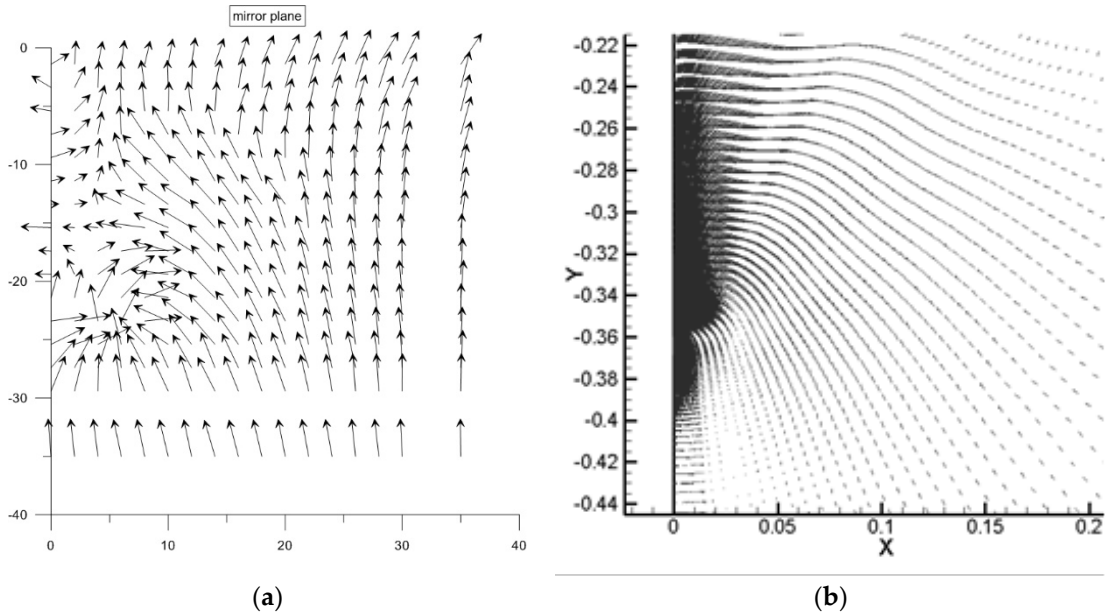

Figure 7. (**a**) Measured velocity vectors at the transom section; (**b**) Analytical velocity vectors at the transom section.

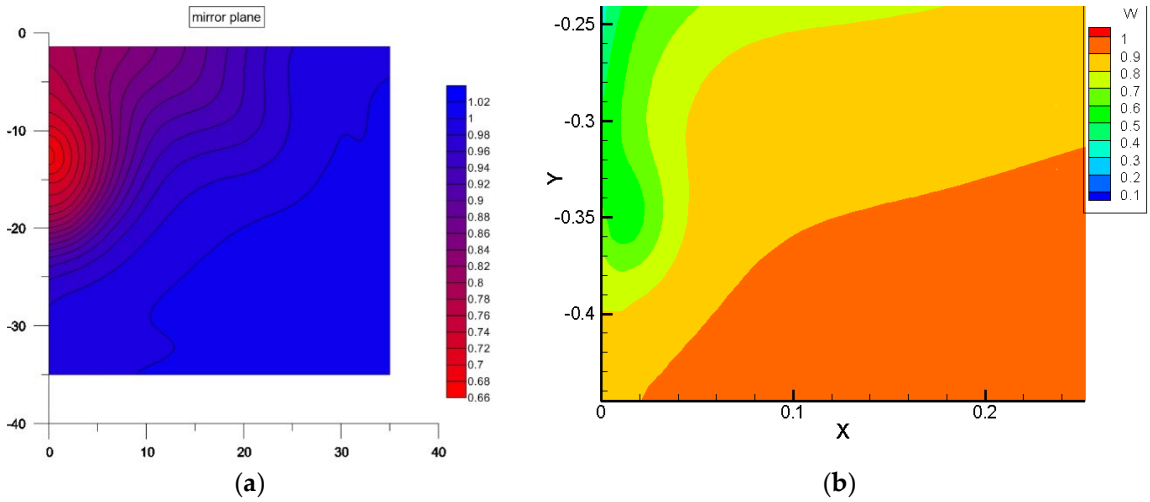

Figure 8. (a) Transom Measured V/Vx; (**b**) Transom CFD V/Vx.

It should be stated that the scaling in the two methods do not match perfectly. Thus, the vortices measured at depths ranging between 12 and 20 cm correspond to the numerical results at depths in the 32 and 40 cm range. It seems that both methods predicted reliably the locations of the vortices.

 doi:10.20944/preprints202604.0010.v1

This can be also observed from the iso-contours were the two methods derived similar results. An attempt to define the center of the vortices is presented in the graph of Figure 9, illustrating the flow direction.

In this figure, the center of the dyne is located at a depth of 36 cm and 3 cm athwartships that corresponds to 16 cm below the water surface. The two methods couldn't be compared directly since a denser grid was needed in the experimental method. However, the appearance of vortices in that section is expected due to intense geometry alternations.

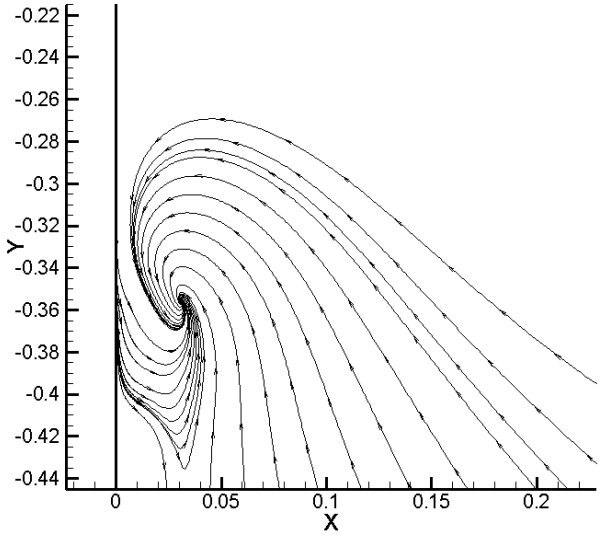

Figure 9. Direction of the Dynes.

7.2. Propeller Plane Section

The second section measured was located at the propeller plane which was about 20 cm forward of the transom. The selected propeller for this vessel has a diameter of 0.1585 m. The grid size was 12 cm in width and 23 cm in depth and the spacing between the points was 1 cm. The starting level of the grid was 2 cm below the model surface at the centerline of the model.

Figures 10a and 10b depicts the velocity vectors of the flow, while Figures 11a and 11b illustrates the iso-contours at the propeller section. On the measured plane at the depth of about 12cm there is an indication of the center of the vortices. A similar situation is predicted by the numerical method at the depth of 34 cm which corresponds to 14 cm below the water surface. The shape of iso-contours derived by both methods are quite similar. On Figure 12 a focused view of the area of the vortex including its center, as derived by CFD, is presented.

 doi:10.20944/preprints202604.0010.v1

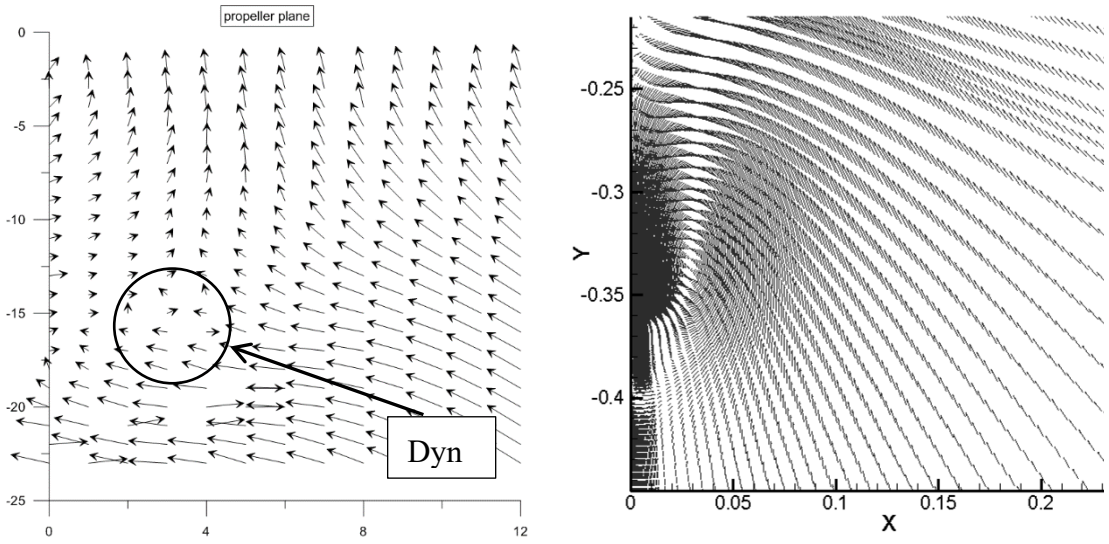

(**a**) (**b**)

Figure 10. (**a**) Measured velocity vectors at the propeller section; (**b**) Analytical velocity vectors at the propeller section.

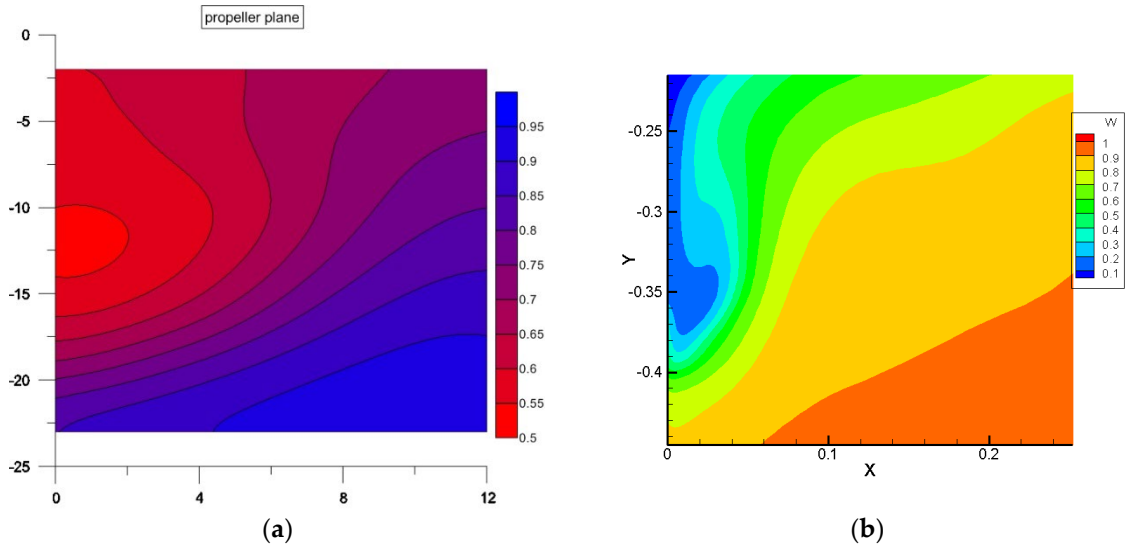

(**a**) (**b**)

Figure 11. (a) Propeller Plane Measured V/Vx; (**b**) Propeller Plane CFD V/Vx.

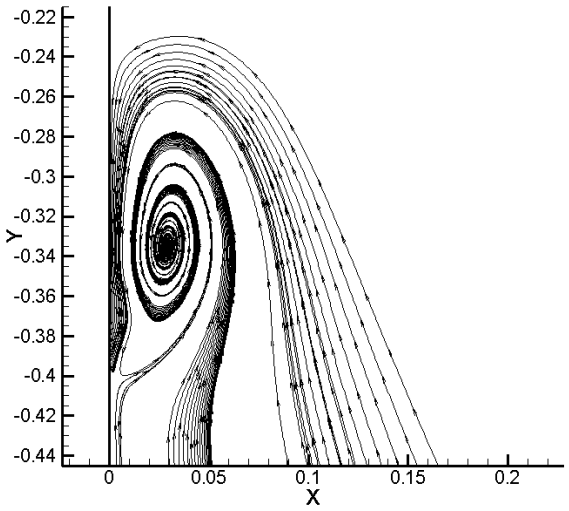

 doi:10.20944/preprints202604.0010.v1

Figure 12. Direction of the Dynes.

7.3. Distance Section

The last section was located 40 cm forward of the transom where there are noticeably changes of the hull shape. At this section the measured grid started at about 1 cm away from the hull, up to 30 cm athwartships and up to a depth of 22 cm. The spacing was 1 cm for the points close to the hull, where large eddies where expected, and increased to 2 cm afterwards.

At the last section, there is no clear sign of a vortex in the flow (Figures 13a and 13b). The two methods seemed to have great similarities with respect to the direction and magnitude of the vectors derived. Based on above results it can be concluded that both methods are in good agreement. Thus, it can be stated that the experimental apparatus is capable to capture the vortices produced at the stern of ship models. The experimentally recorded velocities were in the range of 2 cm/sec up to 1 m/sec. The discrepancies between the numerical and the experimental method were less than 5%.

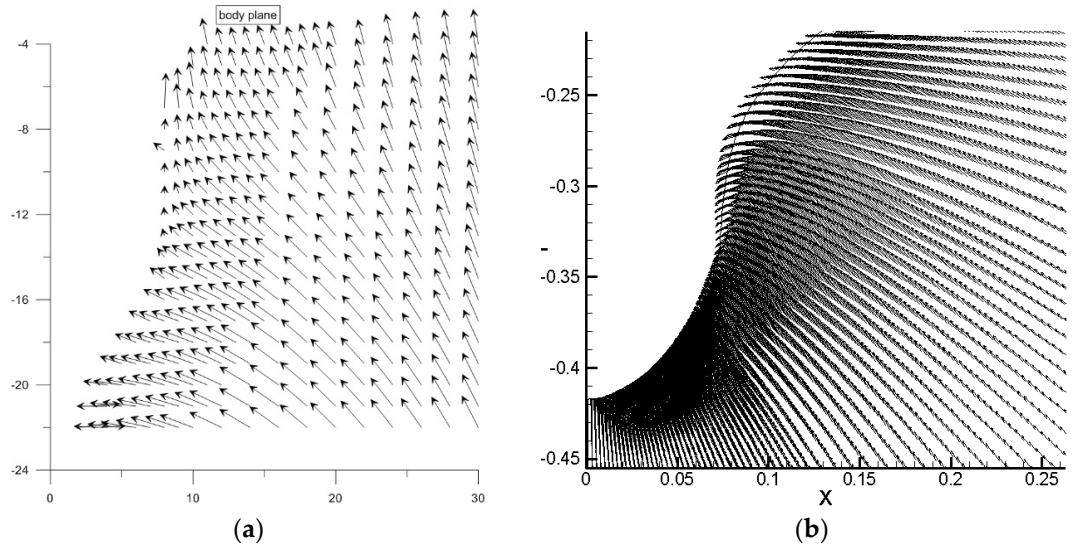

(**a**) (**b**)

Figure 13. (**a**) Measured velocity vectors at the propeller section; (**b**) Analytical velocity vectors at the propeller section.

8. Conclusion

In this paper a contemporary arrangement for accurate measurements of the wake flow at the stern region of a large-displacement ship models is presented. The results were used for the validation of ship flows prediction by an in-house developed CFD code. The experimental arrangement consisting of custom pressure sensors, an accurate traversing system and a five-hole Pitot tube was specifically designed to meet the experimental requirements of the towing tank of LSMH. The results revealed that the longitudinal velocity component has been accurately determined, resulting on accurate and reliable flow field capturing the stern region of ship models at the towing tank of NTUA. However, the transverse velocities were relatively small compared to the axial velocities, resulting in higher overall errors. Long recording time was selected to reduce the effect of vibrations and small carriage speed alterations to improve the measurements accuracy.

The proposed double calibration method, both on air and water flows, considers small misalignments, the selection of the pressure sensors and tubing, geometrical imperfections and experimental conditions, increasing the overall accuracy substantially. A detailed guide for developing a pitot-based measuring system at towing tanks is provided for those who are interested in developing such measurements. The analysis of the velocity field revealed interesting features of the flow field at the stern of the ship, where vortices appear at the section of the propeller and under the transom, where intense alterations of the hull shape occur even in the absence of the propeller.

 doi:10.20944/preprints202604.0010.v1

Both methods seemed to be very good in agreement, capturing the vortices at about the same location, verifying the robustness of the two methods.

Funding: "This research received no external funding".

Data Availability Statement: This work was part of the PhD thesis of the first Author conducted at the Laboratory for Ship and Marine Hydrodynamics under the supervision of the second Author. All CFD results were conducted by the third Author. All the data can be found on the PhD thesis publish on 2020, entitled "Use of laser and PIV techniques to evaluate the resistance and the flow field at the wake of ship with large block coefficient". All the work is property of the NTUA. Further inquiries can be directed to the corresponding author(s).

Acknowledgments: Special acknowledgements must be given to the personnel of the laboratory of Ship and Marine Hydrodynamics for their endlessly efforts for the completion of the project. Especially, the authors acknowledge the contribution by Mr. G. Milonas and J. Trachanas for their contribution on the design and competition of the experiments.

Conflicts of Interest: "The authors declare no conflicts of interest".

References

1. Farkas, A.; Degiuli, N.; Martic, I.; Dejhalla, R. 2018, Numerical Assessment of Nominal Wake for a Bulk Carrier**.** *Journal of Marine Science and Technology* **2018**, 24, pp. 1092-1104.
2. Liarokapis, D.; Zarifis, A.; Trachanas, J.; Tzabiras, G. Experimental Investigation of the Wake Flow of a Bulk-Carrier Model Using a Five-Hole Pitot Arrangement. In Proceedings of the 2nd International Conference on Maritime Technology and Engineering, Lisbon, Portugal (AMT), 15-17 October 2014. DOI: 10.1201/b17494-118.
3. Liarokapis, D.; Grigoropoulos, G.; Perissakis, S. Introducing a Seven-hole Pitot Arrangement for Measuring Wake Flows in the Towing tank. In Proceedings of the 1st International Conference on Advanced Measuring Technology for the EU Maritime Industry (AMT), Nantes, France, 1-2 September 2009.
4. Gui, L.; Longo, L.; Stern, F. Towing Tank PIV Measurement System, Data and Uncertainty Assessment for DTMB Model 5512. *Journal Experiments In Fluids* **2001**, 31, pp. 336-346. DOI:10.1007/S003480100293.
5. Lee, S.J.; Koh, M.S.; Lee, C.M. PIV Velocity Field Measurements of Flow Around a KRISO 3600TEU Container Ship Model. *Journal of Marine Science and Technology* **2003**, 8, pp. 76–87. DOI:10.1007/s00773-003-0156-4.
6. Lee, J.Y.; Paik, B.G.; Lee, S.J. PIV Measurements of Hull Wake Behind a Container Ship Model with Varying Loading Condition. *Journal of Ocean Engineering* **2009**, 36, pp. 377–385. DOI:10.1016/J.OCEANENG.2009.01.006.
7. Wu, T.; Luo, W.; Jiang, D.; Deng, R.; Li Y.; Stereo Particle Image Velocimetry Measurements of the Wake Fields Behind A Panamax Bulker Ship Model Under the Ballast Condition. *Journal of Marine Science and Engineering* **2020**, 8(6), pp. 397. DOI:10.3390/jmse8060397.
8. Maksoud, A.; Brandt, H.; Nowacki, H.; Tzabiras, G. An Experimental and Numerical Investigation of Turbulent Flows Around a Ship-like Body with and without Propeller, In *WIT Transaction on the built Environment*, WIT Press, 1995, Vol. 11, pp. 99–113, ISSN: 1743-3509.
9. Hoekstra, M.; Ligtelijn, I. Micro Wake Features of a Range of Ships. MARIN Report 410461-1-PV, 1991, Maritime Research Institute Netherlands, Wageningen, The Netherlands.
10. Longo, J.; Huang, H.; Stern, F. 1998, Solid/Free Surface Juncture Boundary Layer and Wake. *Journal Experiments in Fluids* **1998**, 25, pp. 283–297. DOI: 10.1007/s003480050232.
11. Tzabiras, G.; Psaras, K. Numerical Simulation of Self-Propulsion Tests of a Product-Carrier at Various Conditions. In Proceedings of the 9th International Conference on High-Performance Marine Vehicles (HIPER), Athens, Greece, 3-5 December 2014.
12. Tzabiras, G.; Tserpes, H.; Polyzos S.; Liarokapis D. On the Computation of the Propulsive Characteristics of a Tanker. In Proceedings of the 5th International Conference on Maritime Technology and Engineering (MARTECH), Lisbon, Portugal, 16-19 November 2020, DOI: 10.1201/9781003216599-13.

 doi:10.20944/preprints202604.0010.v1

13. Robinson, A.; Butterfield, D.; Curtis, D.; Thompson, T. Problems with Pitots. Issues with Flow Measurement in Stacks. In Proceedings of the 6th International Conference on Emission Monitoring, Milan, Italy, 9-11 June 2004.
14. Pisasale, A.; Ahmed, N. Examining the Effect of Flow Reversal on Seven-Hole Probe Measurements. *Journal of American Institute of Aeronautics and Astronautics* **2003**, 41 (12), pp. 2460-2467, DOI: 10.2514/2.6845.
15. Pisasale, A.; Ahmed, N. Development of a Functional Relationship Between Port Pressures and Flow Properties for the Calibration and Application of Multihole Probes to Highly Three-Dimensional Flows. *Journal Experiment in Fluids* **2004**, 36, pp. 422-436. DOI: 10.1007/s00348-003-0740-8.
16. Zilliac, G. Modelling, Calibration, and Error Analysis of Seven-Hole Pressure Probes. *Journal Experiment in Fluids* **1993**, 14, pp. 104-120.
17. Telionis, D.; Yihong, Y. Recent Developments in Multi-Hole Probe (MHP) Technology. In Proceedings of the 20th International Congress of Mechanical Engineering, Gramado, Brazil, November, 15-20 November 2009.
18. Tzabiras, G. A Method of Predicting the Influence of an Additive Bulb on Ship Resistance. In Proceedings of the 8th International Conference on Hydrodynamics (ICHD), Nantes, France, 30 September – 3 October 2008.
19. Tzabiras, G.; Polyzos, S. A hybrid numerical method for calculating self-propulsion characteristics of ships. In Proceedings of the International Conference of Maritime Association of the Mediterranean (IMAM), Pula, Croatia, 21-24 September 2015.
20. Tzabiras, G.; Kontogiannis K. An Integrated Method for Predicting the Hydrodynamic Performance of Low CB Ships, *Journal of Computer Aided Design* **2010**, 4, pp. 985-1000.
21. Tzabiras, G. Resistance and self-propulsion simulations for a Series-60, CB=0.6 hull at model and full scale. *Journal of Ship Technology Resistance* **2004**, 51, pp. 21-34. DOI:10.1179/str.2004.51.1.004.
22. Menter, F. Zonal two equation turbulence models for aerodynamic flows. In Proceedings of the 23th Fluid Dynamics, Plasmadynamics, and Lasers Conference, AIAA 93-2906, Orlando, Florida, 6-9 July 1993. DOI:10.2514/6.1993-2906.
23. Polyzos, S,; Tzabiras, G. On the Calculation of Propulsive Characteristics of a Bulk-Carrier Moving in Head Seas. *Journal of Marine Science and Engineering* **2020**, 8(10), pp. 786, DOI:10.3390/jmse8100786.
24. Gerner, A.; Mauer, C.; Gallington, R. Non-nulling seven-hole probes for high angle flow measurement. *Journal Experiment in Fluids* **1984**, 2, pp. 95-103.
25. Venkateswara Babu C,; Govardhan, M,; Sitaram, N. A method of calibration of a seven-hole pressure probe for measuring highly three-dimensional flows. *Journal of Measurement Science and Technology* **1998**, 9, pp. 468–476. DOI:10.1088/0957-0233/9/3/022.
26. Zilliac, G. 1989, Calibration of Seven-Hole Pressure Probes for Use in Fluid Flows with Large Angularity, NASA Technical Memorandum 102200, December 1989.
27. Nowack, C.F.R. Improved calibration method for a five-hole spherical probe. *Journal of Physics E: Scientific Instruments* **1970**, 3, pp. 21-26.
28. Longo, J,; Stern, F. Uncertainty Assessment for Towing Tank Tests With Example for Surface Combatant DTMB Model 5415. *Journal of Ship Research* **2005**, 49(1), pp. 55–68. DOI: 10.5957/jsr.2005.49.1.55.